

Effect of ball-milling time on mechanical and magnetic properties of carbon nanotube reinforced FeCo alloy composites

Amar J Albaaji^{1*}, Elinor G Castle^{2,3}, Mike J Reece^{2,3}, Jeremy P Hall¹, Sam L Evans⁴

1-Wolfson Centre for Magnetics, Cardiff School of Engineering, Cardiff University, UK

2-School of Engineering and Materials Science, Queen Mary University of London, UK

3-Nanoforce Technology Ltd., London, UK

4-Institute of Mechanical and Manufacturing Engineering, Cardiff School of Engineering, Cardiff University, UK

*Corresponding author at: Wolfson Centre for Magnetics, Cardiff School of Engineering, The Parade, Cardiff University, Cardiff CF24 3AA, UK.

College of Engineering, Al-Qadisiyah University, Iraq.

Tel. +44(0)7440731570; Fax: +44 02920874716; E-mail address: amar.jabar@yahoo.com

School of Engineering and Materials Science, Queen Mary University of London, Mile End Rd, London E1 4NS, UK.

Nanoforce Technology Ltd., Joseph Priestley Building, Queen Mary, University of London, Mile End Road, London E1 4NS, UK.

Institute of Mechanical and Manufacturing Engineering, Cardiff School of Engineering, Cardiff University, The Parade, Cardiff University, Cardiff CF24 3AA, UK.

Key words: Ball milling, carbon nanotube, Spark plasma sintering

Abstract

Carbon nanotubes (CNTs) reinforced FeCo alloys were produced by high energy ball-milling and spark plasma sintering (SPS). CNTs distribution in the FeCo alloy was gradually improved as ball-milling time increased, with a uniform dispersion achieved after 6 h ball-milling. Tensile tests demonstrated that, as the ball-milling time increased, the yield strength increased in the composites; a maximum 50 % relative increase in tensile strength due to the addition of CNTs was achieved after 1 h ball-milling, which then decreased with further ball-milling. The elongation to fracture was significantly increased after 1 h ball-milling and then decreased with further ball-milling. SEM results show a patch of dimples in the fracture surface of the composite, indicating improved ductility due to CNTs. The coercivity was increased with increased ball-milling time, while the saturation induction showed a peak value after 1 h of ball-milling and then decreased with further ball-milling. Raman spectra of the composite indicated that no serious damage had been imparted to the CNTs during ball-milling.

1. Introduction

Equiatomic FeCo alloy is one of the most important soft magnetic alloys in electromagnetic technology due to its high saturation magnetisation, high Curie temperature, and high flux density [1]. There is increasing interest in replacing hydraulic and pneumatic systems in aircraft by electromagnetic actuators, requiring soft magnetic alloys with an ideal combination of high saturation induction (> 2 Tesla) and yield strength of 600 MPa or higher at 600 °C [2]. However, whilst FeCo alloy offer excellent magnetic performance, there are significant limitations in its mechanical behaviour such as extreme brittleness. Composite

strengthening may offer improved mechanical properties such as higher strength, improved ductility and stability at high temperatures and due to less compromise between the components, the deterioration in magnetic properties will be less in the soft magnetic matrix alloy.

Carbon nanotubes can provide an ideal reinforcement in composite materials; owing to their unique mechanical and thermal properties, high aspect ratio, large surface area and low density [3, 4, 5]. However, the full potential of CNTs as the reinforcing phase has not been realised yet, due to the inherent challenge in obtaining uniform dispersions and good quality matrix-reinforcement interfaces. In order to improve dispersion of carbon nanotubes in metal matrices, functionalization of the carbon nanotubes was trialled [6], using an acidic treatment and dispersion in a liquid medium through ultrasonic agitation. However, only a limited volume fraction of CNTs were dispersed uniformly on the surface of the powder particles, leading to a limited improvement in mechanical properties [7]. Additionally, low energy ball-milling steps did little to improve the CNT dispersion in FeCo alloy [8, 9]. However, mechanical alloying by high energy ball-milling has been shown to improve the dispersion of nano-materials in metal matrices. Mechanical alloying (MA) is a powder metallurgy technique which involves a repeated welding, fracturing and rewelding of powder particles during solid-state processes in a high energy ball-mill [10]. This process was first employed in the 1960s by Benjamin [11] to produce homogeneously dispersed oxide nanoparticulates-metal composite powders; following a failure of the reinforcement coating to produce uniform dispersion for reinforcement in metal matrix. The technique was originally developed to improve the properties of nickel -and iron-based super alloys, which were used in aerospace applications [12].

A uniform dispersion of CNTs in metal powder was achieved by Esawi and Morsi [13] using mechanical alloying. Here, the structure of the CNTs remained intact even after intensive ball-milling. A dispersion of CNTs in soft magnetic Ni-Fe alloys has been studied by Azadehrajbar et al [14]; however, in spite of the high pressure (300 MPa) employed in cold compaction and the long (1 h) dwell time at 1040 °C during sintering, the fraction of porosity in the consolidated materials was considerably high. No magnetic or mechanical properties were reported in this study relating to the effect of the addition of CNTs.

So far there has been no systematic study into the effect of high energy ball-milling on FeCo and FeCo/CNT composites. The presented work therefore, aimed to evaluate the

effect of high energy ball-milling time on quality and dispersion of CNTs in FeCo alloy, and to optimise the best ball-milling time to achieve better combination between mechanical and magnetic properties. To improve the interfacial bonding with less reaction with the reinforcement, the sintering processes were performed by SPS.

2. Experimental work

2.1. Starting materials

CNTs were provided by Haydale Ltd., which were functionalized by plasma treatment to incorporate an oxide group covalently bonded to the surface of the CNTs. Gas atomised Fe-50Co-0.2Si alloy powder was supplied by Sandvik Osprey Powder Group. The mean size of the powder, measured by a Malvern Mastersizer 3000 with laser scattering, was 23.4 μm .

2.2. High energy ball milling

High energy ball-milling processes were performed using a planetary ball-mill machine (Fritsch Pulverisette 5 Germany). An 80 ml tungsten carbide jar, with hardened steel balls of $\text{Ø}=10$ mm, were used for the ball-milling processes. The jar and milling media were charged with 20 g of gas atomised FeCo powder under argon gas atmosphere to avoid oxidation. The used ball to powder ratio (BPR) was $\sim 6:1$. To avoid exaggerated cold welding of the powders, 6 ml of isopropanol alcohol was used as process control agent (PCA). A rotation speed of 250 r. p. m. was employed, with 30 min milling and 15 min pause to reduce overheating of the powder. In order to obtain a homogenous dispersion of CNTs, while minimising damage to them, the maximum allowed ball-milling time was 6 h. Samples were extracted following different periods of milling (0.5, 1, 2, 4, 6 h). The resulting slurries were then dried on a hot plate at heating temperature of 120 $^{\circ}\text{C}$ for 5 h.

2.3. Powder consolidation

A spark plasma sintering SPS furnace (HPD 25/1 FCT, Germany) was used to consolidate 20 g of FeCo alloy powders and composite powder mixtures. The powdered samples were loaded onto a $\text{Ø}=20$ mm graphite die lined with graphite foil and manually pre-pressed to 7 MPa using a Specac hydraulic pressing system. The prepared die was then loaded into the SPS furnace, where the process was carried out under 5 Pa vacuum. A pressure of 50 MPa was applied to the die at room temperature and maintained constant throughout sintering. A heating rate of 50 $^{\circ}\text{C min}^{-1}$ was used to increase the temperature to 1100 $^{\circ}\text{C}$, where sintering was performed without dwelling. After fast cooling in contact with the water cooled pistons

of the spark plasma sintering furnace, the compacts were extracted from the die using the hydraulic press.

2.4. Characteristics analysis

The structure of the raw CNTs was evaluated using a high-resolution Transmission Electron Microscope (TEM) (JEM-2100 LaB6). The dispersion of the CNTs in the milled powders was examined using Scanning Electron Microscopy (SEM) (Oxford Instrument). In order to measure the density of synthesised materials accurately, silicon carbide papers of different grades were used to remove the remaining graphite layer from the surface of sintered materials. Density measurements were then performed using the Archimedes' immersion technique in water.

The variations in powder morphology during ball-milling were studied by SEM. To evaluate the dispersion of the CNTs and the interface bonding in FeCo alloy, the microstructure was studied by SEM, in which cross sections of the sintered material were prepared by standard metallographic techniques and etched using 10 % Nital for 30 sec. SEM was also used to examine the fracture surfaces of tensile samples. TEM was used to track the formation of a nanocrystalline structure during ball- milling.

X-Ray Diffraction (XRD) (Philips PW 3830 Automated Powder Diffraction) fitted with a Co target X-ray tube was used to analyse the crystallographic phases and ordering states present in the as-received and composite materials. A wide range of scan angles between 10 and 110 °2θ was selected to evaluate the phases present in the FeCo alloys, at a scan speed of 8×10^{-3} °2θ sec⁻¹, operation voltage 35 kV and current 40 mA. A slower scan 25×10^{-5} °2θ sec⁻¹ at operation conditions of 42 kV and 40 mA was used during a scan over a narrow range, to detect the ordered phase in the expected °2θ range. To assess any damage induced in the CNTs during ball-milling and sintering, the composites were subjected to Raman spectroscopy (Renishaw inVia Raman microscope). All samples were investigated using an excitation wavelength of 514 nm, a power of 25 mW and a spot size of 5 μm. The Raman spectra curves were obtained after scans between 1000 and 3200 cm⁻¹ for 15 accumulations.

2.5. Mechanical and magnetic properties

Tensile tests were performed following BS EN 10002-1:2001 standard. Three tensile samples of dimensions 11 × 3 × 1.25 mm were cut from the 30 mm diameter monolithic FeCo alloy

and composite discs by electrical discharge machining (EDM). In order to remove any crack initiation sites introduced by the cutting process, the samples were ground using silicon carbide papers. A cross head speed of 2 mm min^{-1} was used for all tensile tests using a Shimadzu machine. Hardness measurements for both the base FeCo alloy and composites were performed in five different locations using a Vickers hardness tester to apply a 30 g load for 4 sec.

DC magnetic tests were performed on an automatic universal measurement system; sweeping the magnetic field up to 25 kA m^{-1} . Rectangular specimens of dimensions $24 \times 5 \times 2.5 \text{ mm}$ were cut from the compacted 30 mm diameter discs using EDM and used to perform the magnetic tests after polishing to remove surface roughness from cutting.

3. Results and discussion

3.1. Raw materials

The morphologies of the raw FeCo and CNT materials are shown in Fig.1. A spherical morphology with a wide particle size distribution is observed in the as received FeCo alloy. The entangled CNT clusters exhibit a variation in the tube diameters and in the number of layers. Damage has been observed on the surface of some of these tubes, as shown by the arrows.

3.2. The SEM morphology of milled FeCo alloy and composite powders

The SEM morphology of the ball-milled FeCo alloy and composite powders are presented in Fig.2. The diameters of particles were measured by Image J software and presented in Table 1. The morphology of FeCo powder was altered during the ball-milling process. The spherical shape of the as received FeCo powder was deformed into plate-like particles after 0.5 h milling, while the variations in particles size were broad, with little particle welding occurring during this time. Increasing the ball-milling time to 1 h led to a broader particles size range due to increased plastic deformation and more welding between powder particles. The welding processes increased as the time increased and became significant after 4 and 6 h of ball-milling. In the composite powder, ball-milling up to 0.5 h was not effective in dispersing the CNTs; bundles of carbon nanotubes were observed between and on the surface of particles. Extending the time to 1 h increased the size of the FeCo particles with improved CNT dispersion on the particle surface and some evidence for the embedding of CNTs into the particles. Significant welding of FeCo particles began after 2 h ball-milling, in which

small particles were welded onto larger ones. As a result, almost all the carbon nanotubes were embedded into the FeCo alloy particles at this milling time. After 6 h the surface of the particles became very smooth and no free carbon nanotubes could be seen. Adding CNTs to the monolithic FeCo alloy powder altered the powder behaviour during the ball-milling process, leading to a reduction in particle size Fig. 2. This can be attributed to an increase in the fracture rate due to the embedded CNTs, which increase the hardness and brittleness of the particles. The fractured particles were observed after 4 h ball-milling time in the composite material, while the welding process was observed in the monolithic FeCo alloy at this time (Fig.2). The CNT clusters acted as a lubrication barrier against welding between the powder particles during the initial stage of dispersion, after shortening of the CNTs by ball-milling [15], the barrier was gradually removed, and CNTs were embedded inside the particles during cold welding, leading to increase in the strain hardening rate in the deformed particles [13].

3.3. Effect of ball milling on densification and density of the consolidated materials

SPS shrinkage curves of the as received FeCo alloy, ball-milled monolithic FeCo alloy and 1.5 vol.% CNTs composite are presented in Fig. 3. A difference is observed in the curves between the three materials. This can be attributed to the difference in powder composition and morphology, due to the different levels of plastic deformation experienced during the ball-milling process. There is a shift in the sintering curve to lower temperatures for the ball-milled FeCo and composite powders, as compared to the as received FeCo alloy. This can be attributed to the effect of ball-milling, which introduced a higher dislocation density to the material and therefore a higher strain energy compared to the as received FeCo alloy; lowering the activation energy for sintering. Densification occurred over a broader temperature range for the ball-milled monolithic FeCo alloy and 1.5 vol.% CNT composite compared to as-received FeCo alloy as confirmed from broadening in shrinkage curves. Increasing ball-milling time to 6 h increased the degree of agglomeration in the monolithic FeCo alloy and 1.5 vol.% CNT composite powders Fig.2. These agglomerations made sintering of ball-milled powder rather more difficult than for as-received powder [16]. Extending the milling time to 6 h, lead to a decrease in density of both consolidated monolithic FeCo alloy and 1.5 vol.% CNT composite Fig. 4. However, the relative density of the composite material was higher than that of the monolithic FeCo alloy. This may be due to the role of the CNTs in decreasing agglomeration in the powder during milling Fig. 2. The highest relative density of 100 % was achieved after a milling time of 1 h for the 1.5 vol.%

CNT composite, suggesting that the morphology of the powder at this time was more suitable for consolidation under the sintering pressure of 50 MPa.

3.4. Microstructure of consolidated materials

SEM microstructure images of the consolidated materials are shown in Figs. 5 and 6. The measurements of grain size by ImageJ software are shown in Table 2. It can be seen that CNT agglomeration was reduced with increasing ball-milling time Fig. 6. A uniform dispersion of CNTs was observed after 6 h ball-milling time in which the CNTs were embedded into the grains. The grain size was significantly refined in FeCo alloy after ball-milling and also after embedding CNT in FeCo alloy. Unfortunately, the consolidated materials exhibit porosity, which can be attributed to the agglomeration occurring in the composite and monolithic FeCo alloy powders after ball-milling to 6 h. Employing a 50 MPa sintering pressure was not sufficient to break down this agglomeration during sintering. However the agglomeration was reduced in the composites and hence the density was improved. Adding CNTs to the FeCo alloy reduced the grain size due to the increased strain hardening, and subsequently, fracturing rates occurring in FeCo particles as the CNTs become embedded within the particles during ball-milling. Furthermore, grain growth was inhibited by the presence of CNTs during the sintering process. Both of these factors caused a refinement in the microstructure of the composite materials in comparison to monolithic FeCo alloy.

3.5. X-ray diffraction (XRD) analysis

XRD analysis of the as received, ball-milled monolithic FeCo alloy and 1.5 vol. % CNT composites processed at different ball-milling times of 1, 4, and 6 h are presented in Fig. 7. XRD diffraction patterns of a slow scan analysis in the range of the expected superlattice lines for the aforementioned materials are also shown in Fig. 8. All the detected peaks were referenced to standard data (JCPDS); (00-044-1433) of the FeCo alloy, (01-082-1395) of silicon oxide, (00-003-0400) of iron carbide and finally carbon nanotube and carbon according to (03-065-6212) taking into account the wave-length of the Co tube ($\lambda=1.78896$ Å).

Oxidise was included in the as-received powder due to exposure to air, as confirmed from the silicon oxide peaks which were present prior to milling. Moreover, carbon was already present (Fig.7) in the as received FeCo alloy as a result of the fabrication processes used. In order to check the interaction between the FeCo alloy and the CNTs during ball-

milling, the XRD profile was enlarged as shown in the inset in Fig. 7. The intensity of the carbon peak was increased in the 1.5 vol. % CNT composite, as would be expected from including CNTs. Very low-intensity peaks of iron carbide were observed, which were also formed in the monolithic FeCo alloy. However, the slight increase in the intensity of the carbide peaks in the composite materials can be attributed to the reaction with the amorphous carbon in the CNTs. The TEM work showed that amorphous carbon was present on the surface of the as-received CNTs (Fig.1), hence this may not be an artefact of the milling process. It has been reported by Kuzumaki et al. [17] that the CNTs are stable and do not react with the metal matrix alloy as long as their quality is high and the level of defective tubes is low.

The crystallite size and lattice strain due to dislocation concentration can be evaluated from the peak broadening in the XRD profile [18]. The effect of strain on the d -spacing may be classified as uniform and nonuniform. Peak position is very sensitive to uniform strain while peak broadening and intensity are affected by nonuniform strain [19]. The shift in the diffraction lines of the XRD corresponds to strains induced in the materials.

A nanocrystalline structure was formed during ball-milling, as confirmed by TEM observation Fig.9. As well as TEM imaging, the crystallite size can be estimated using the Scherrer method, which relies on X-ray profile analysis. The anti-phase domain size was measured using this method for the superlattice line (100). The APDS was decreased with extended ball-milling time in the monolithic FeCo alloy, becoming 22.48 nm after 6 h ball-milling. In the 1.5 vol. % CNT composite, a maximum APDS of 34.27 nm was observed after 6 h ball-milling time. This might be due to the lubricating role played by the CNTs during ball-milling, which reduces the intensity of the impact of ball-milling on the crystallite structure. The highest intensity value of the superlattice line (100) was observed after an extended milling time of 6 h for both the monolithic FeCo alloy and the 1.5 vol. % CNT composite. Introducing CNTs to the FeCo alloy increased the volume fraction of the ordered structure in the composite compared to the monolithic FeCo alloy [8]. Up-shifting was observed for both the monolithic FeCo alloy and the 1.5 vol. % CNT composites, as confirmed from the increasing diffraction angle with ball-milling time Fig. 8. A slight increase in peak shifting is seen in the composites as compared to the monolithic alloy, corresponding to the increased value of strain hardening in composites from embedded CNTs into the FeCo particles.

3.6. Structural integrity of CNTs

Raman spectroscopy is a popular tool for the characterization of the structure and properties of carbon nanostructures [20]. The quality of the raw CNTs and the 1.5 vol. % CNT composites was evaluated using Raman spectroscopy, as shown in Fig. 10. One characteristic feature of single-walled carbon nanotube (SWNT) observed by Raman spectroscopy is the splitting of the G band. The raw CNTs employed were a multiwall carbon tube (MWCNT). The absence of any splitting in the G band in MWCNTs compared to the large splitting in the G band to G^+ - G^- for small diameter SWNT tubes is due to the large diameter of the outer tubes and variation in diameter distribution within the individual MWNTs, which are considered to be an assembly of diameters ranging from small to very large [21]. The reason behind the splitting in the G band is the difference in the sources of vibration observed during the Raman spectroscopy test. G^+ is associated to vibration frequencies occurring along the tube axis while the frequencies that result from vibration along the circumference of the tube lead to G^- [22].

However, it is possible to observe a clear splitting in the G band in multiwall CNTs prepared by hydrogen arc discharge, which contain a small innermost diameter [23]. This was attributed to the effect of environment, which becomes relatively small for the innermost nanotube compared to interactions between SWNTs which occurred in different environments [21]. The splitting decreased as the outer diameter of the carbon nanotubes increased. The wall layers in the CNTs were decreased after ball-milling, as shown from splitting in the G band of the Raman spectra. Slippage between shells and thinning of the CNTs occur during ball-milling, leading to a reduced diameter in the CNTs at extended milling time, leading, eventually to the observation of splitting in G-band.

The nature of the interfacial bonding between the carbon nanotubes and the matrix material can influence the lattice vibrations of the CNTs, causing a shift in the Raman spectra. A detailed study on the correlation between transferred tensile stresses and G peak position has been reported in [24]. A downshift was observed in the split G bands and this shifting was higher in the sample ball-milled for the full 6 h. This could be due to the fact that the interfacial bonding between the CNTs and the matrix alloy had improved, allowing more stresses to be transferred from the FeCo matrix to the CNTs, or due to the increased heat and stresses encountered during the longer ball-milling times. It is not possible here to ignore the effect of stresses from ball-milling in the observed shifting. The intensity ratio R (I_D / I_G) is usually used to characterise the damage in the CNTs. The calculated ratios of the consolidated materials are presented in Table 3. The intensity ratio (R) decreased in the

consolidated materials for all ball-milling times in comparison to the as-received CNTs. There are two possible reasons for this improvement in CNTs quality after fabrication. The first is attributed to releasing the functional oxide group during the sintering processes; and the second is the purification of CNTs due to slippage of the outer shells during the ball-milling process. It can be seen that the R ratio increased with increasing ball-milling time reflecting the increased damage done to the CNTs during ball-milling. However the highest value of the R ratio for the ball-milled samples is still significantly lower than for the as received CNTs (Table 3). Therefore, while some damage was induced by ball-milling, this was minimal and was far outweighed by the positive effects of the corresponding improvement in CNT dispersion.

3.5. Magnetic properties

A summary of the magnetic properties measured for the consolidated materials is shown in Fig.11. The saturation induction decreased after ball-milling the monolithic FeCo alloy and 1.5 vol. % CNT composite materials in comparison to the as-received FeCo alloy; peak saturation values were 2.35 T and 2.33 T after a milling time of 1 h for the monolithic FeCo alloy and 1.5 vol. % CNT composite materials respectively. The lowest values of coercivity were observed after 0.5 h of ball-milling; giving values of 511 A/m and 573.5 A/m, which were increased to 1335 A/m and 1248 A/m after 6 h ball-milling for the monolithic FeCo alloy and 1.5 vol. % CNT composite respectively. The coercivity value was lower in composite materials as compared to the monolithic FeCo alloy at ball-milling times of 4 and 6 h as shown in Fig. 11.

The permeability and coercivity of magnetic materials are very sensitive to microstructure changes, strains, and presence of impurities [25]. Despite the increases in intensity of the ordered state, which reflects increase in amount of ordered phase in structure and also the increase in the density of the 1.5 vol. % CNT composite materials (Figs.4 and 8) with extending ball-milling time, the saturation induction was decreased in composite materials. XRD results show more broadening and shifting in the composite materials in comparison to the monolithic FeCo alloy Figs. 7 and 8. This can be attributed to the increased strain hardening occurring in the composite materials owing to the embedding of CNTs in the FeCo particles. Stains are included during fabrication processes, which are different in their magnitude and direction in microstructure. Therefore, magnetoplastic anisotropy will form due to obstacle domains walls movement, which cause decrease in permeability, and increase

in coercivity, [25, 26]. As result of decreasing in permeability the saturation induction will be effected and higher magnetic field is required to achieve saturation induction. Furthermore, inclusions have a dilution influence on magnetization, the inclusions were included in microstructure from reaction with metallic catalyst on surface of raw CNTs during fabrication Fig.1 [27], or from carbon result from damage CNTs during ball-milling. Formation of carbide in microstructure was confirmed from X-ray diffraction Fig. 7. Increasing the amount of carbide combined with the decrease in relative density as the ball-milling time was caused led to a decrease in saturation induction with ball-milling the time.

More strains were included in microstructure, which were not relived by zero dwelling time during sintering, and more contamination from ball-milling medium which is beyond the sensitivity of the XRD technique led to increase in coercivity with further ball-milling time. The microstructure observations showed that the structure was refined as the ball-milling time increased Fig. 5. It is well known that the coercivity is inversely proportional to the grain size, indicating that the fine microstructure has also contribute to the highest values of coercivity for both the monolithic FeCo alloy and the 1.5 vol. % CNT composite. Moreover, the density was decreased with increasing ball-milling time due to agglomeration of the monolithic FeCo alloy and composite powder, which also has promoted the coercivity. Despite of that a decrease in coercivity was observed in 1.5 vol. % CNT composite as compare to monolithic FeCo alloy with further extending in ball-milling time. It was found that the uniform dispersed CNTs in FeCo alloy to cause an increase in saturation induction with reduced coercivity, due to improve densification and formation nanocrystallite ordered structure [28].

3.6. Mechanical properties

The stress-strain curves for the sintered materials are shown in Fig.12. The variations in ultimate tensile strength, yield strength, hardness, and elongation as a function of ball-milling time for the monolithic FeCo alloy and the 1.5 vol.% CNT composites are summarized in (Figs.13, 14 and 15), respectively. Since the CNTs alter the milling behaviour of the FeCo alloy powder, the tensile strength, yield strength, elongation, and hardness of the consolidated FeCo alloy composites are affected accordingly. The highest improvement in ultimate strength due to the addition of CNTs was achieved after 1 h ball-milling time; increasing by almost 50 %. The highest ultimate tensile strength was obtained in the 1.5 vol. % CNT composite after 6 h of milling; giving a value of 611 MPa combined with the highest yield

strength of 536 MPa. The monolithic FeCo alloy exhibited increased ultimate tensile strength and yield strength with increasing ball-milling time. The improved ultimate tensile strength and yield strength in the monolithic FeCo alloy after ball-milling may have been due to the observed refinement in grain size (Fig. 5) and to the increased strain hardening effects as a result of the stresses introduced during ball-milling, which increased with extended ball-milling time.

In the CNT composites the reinforcement improves the mechanical properties through several different physical mechanisms, including thermal mismatch, Orowan looping and shear lag. Detailed explanations of these mechanisms are given by George et al. [29]. These mechanisms are generally related to dislocation density, inhibiting dislocation movement and transferring the load to the reinforcement via the reinforcement-matrix interface. Therefore, the quality of the reinforcement, its dispersion, and the reinforcement-matrix interface bonding are the key parameters for achieving the highest improvement in properties. The trend of ultimate strength with ball-milling time shows a maximum improvement after only 1 h ball-milling time. The quality of the CNTs is directly related to the ball-milling time (Table 3), therefore, the reduced ball-milling time led to less damage in the CNTs. A greatly reduced degree of carbide formation in comparison to the longer ball-milling times may also be playing a part; since the lower concentration of carbide and functionalization groups would provide better sites for improved interfacial bonding. Under controlled conditions, the formation of carbides can have a beneficial effect on the interfacial bonding and on the overall properties [30]. Regarding the effect of density on properties; the density was shown to be reduced with further ball-milling time (Fig. 4.), which has been attributed to alterations in the densification processes occurring due to the changes in morphology and consistency of the powder ball-milled for extended periods of time. As the ball-milling time was reduced to 1 h 100 % relative density was achieved Fig.4. Grain size refinement was higher in the composites as compared to the monolithic FeCo alloy, due to the role of CNTs in inhibiting grain growth Table 2. Microstructural refinement is one of the most important strategies for the improvement of the properties of FeCo alloys. The phase transformation occurring between the ordered and disordered structures has a significant effect on the mechanical and physical properties. Irrespective of grain size, the yield strength and elongation are increased in the disordered Fe₅₀Co as compared to the ordered structure [31]. Further ball-milling time increased the ordered phase, which was increased further as the CNTs become embedded into the FeCo alloy, as shown in (Fig. 8) from increasing the

peak intensity of superlattice line. Therefore, improvements in mechanical properties brought about due to the embedding of CNTs in monolithic FeCo alloy at extended ball milling times have been offset by the increase in volume fraction of the ordered phase

The hardness of the consolidated as-received FeCo alloy was much lower than that of the ball-milled monolithic FeCo alloy and the 1.5 vol. % CNT composites. The hardness increased with increasing ball-milling time in the monolithic FeCo alloy Fig. 14. This difference in hardness after ball-milling is possibly attributed to the high dislocation density introduced to the material and to structural refinement observed in the ball-milled samples. The measurements of crystalline size demonstrate refinement in the monolithic FeCo alloy with further ball-milling time as shown in (Fig.8), accounting for the increased hardness. The hardness of the 1.5 vol. % CNT composites did not scale linearly with ball milling time. The increase in hardness was significant up to 1 h ball-milling time, and then was decreased after 2 and 4 h. After 6 h ball-milling the hardness was decreased in the composite as compared to the monolithic FeCo alloy. Adding CNTs to the FeCo alloy caused further refinement of the microstructure (Fig. 5); and a finer microstructure leads to increased hardness. Moreover, the relative density was higher in the 1.5 vol. % CNT composite compared to the monolithic FeCo alloy (Fig. 4), which will have a significant effect on the hardness. XRD shows an increase in the degree of ordered structure as the ball-milling time was increased and with the introduction of CNTs, as shown in Fig. 8. The hardness was significantly high in the ordered structure compared to the disordered structure. Ordering in the FeCo alloy significantly raises the work hardening rate and reduces elongation [32]. Therefore, the amount of strain hardening was increased as the stresses and the ordered phase were increased with further ball-milling time, leading to the highest value of hardness of 308.2 ± 8.49 VHN and 313.6 ± 5.59 VHN for the 1.5 vol. % CNTs composite and the monolithic FeCo alloy, respectively, after 6 h ball-milling, in spite of the decrease in their relative density Fig.4. Hardness improvement after ball-milling was also reported in [33].

Elongation was significantly increased from 2.82 % in the monolithic FeCo alloy to 6.09 % in the 1.5 vol. % CNT composite when the materials were prepared with the same history of 1 h ball-milling. Elongation then was decreased after 6 h ball-milling for both the FeCo alloy and the 1.5 vol. % CNT composite; but was still higher in the latter than in the former Fig.15. The elongation of the FeCo alloy composite is generally affected by; the ductility of the base alloy, the quality of the reinforcement and its dispersion, the reinforcement-matrix interfacial bonding and the volume fraction of ordered phase.

Optimisation of the ball-milling time is very important to achieve the best dispersion with high interfacial bonding and minimised damage to the CNTs. Ball-milling for 6 h has been reported as the best time for embedding the CNTs inside Al matrix particles without the formation of a carbide and with minimum damage to the CNTs, leading to the highest improvement in tensile strength and mechanical properties [7]. However, the quality of the CNTs, ball-milling conditions, and matrix material must be considered in the optimisation of the ball-milling time. The results show that the highest value of elongation was achieved after 1 h ball-milling time. Different factors contributed to the improved elongation after a limited ball-milling time of 1 h. Firstly, the damage in the CNTs was very low as confirmed in (Table 3), and therefore the formed carbide from reaction with the CNTs was also low at this milling time. The second factor is the powder morphology; this was not significantly affected after 1 h ball-milling time, hence agglomeration was not present and sintering processes were not retarded as in samples with extended ball-milling time. The final density of the compact was therefore improved. Thirdly, since the ball-milling time was short the introduction of impurities by the milling media was minimised. Therefore, the negative effect of impurities on the elongation behaviour was reduced in this composite. Finally, since the elongation of the ordered structure in Fe₅₀Co at room temperature is zero [31], the decrease in the elongation value for both the monolithic FeCo alloy and the 1.5 vol. % CNT composite after 6 h ball-milling was mostly due to the increased ordered structure.

The dominant fracture mode in the FeCo alloy in both the ordered and disordered states is intergranular fracture, due to the inherent weakness in grain boundary bonding [2]. Transgranular fracture was observed for both the monolithic FeCo alloy and the 1.5 vol. % CNT as shown in Fig. 16. This is an indication that an improvement in granular bonding has been achieved in the FeCo alloy using this procedure. However, porosity was noted on the fracture facets; especially for the extended ball-milling time of 6 h, which can be attributed to the effect of agglomeration of the powder on the densification processes. Pull out of single CNTs was observed, with the FeCo alloy being tightly adhered to the surface of the CNT as shown in Fig.17. This indicates that a strong interfacial bonding and uniform dispersion has been achieved by ball-milling. The observed patches of dimples on the fracture surface can be attributed to the improvement in bonding between the FeCo grains and the CNTs, which has significantly improved the elongation in the 1.5 vol. % CNT composite.

4. Conclusions

The conclusions have been drawn from the work are briefly shown as follows: CNTs worked as lubricant during ball-milling, leading to improve densification and to reduce agglomeration in composite powder, however, the completely embedded CNTs and drought the lubricant after 6 h ball-milling caused agglomeration in composite powder. A dual influenced role on quality of reinforcement were played by ball-milling, the first being to cause thinning of the CNTs and the second being to convert the unstable CNT into amorphous carbon. The tensile and yield strength were increased with increasing ball-milling time to 6 h; the highest value for strengthening was achieved after 1 ball-milling time for 50 %, showing a significant increase in elongation as well. The fracture surface showed evidence for strong interfacial bonding by ball-milling. Patches of dimples were observed which are attributed to improved grain boundary bonding by CNTs. The highest values of saturation induction of 2.35 T and 2.33 T in the monolithic FeCo alloy and 1.5 vol. % CNT composite, respectively were achieved after 1 h ball-milling, due to improved density and less amount of formed carbides. However, the coercivity was significantly increased with ball-milling time, owing to grain size refinement and more carbide formation.

Reference

- [1] Sourmail, T., 2005, "Near equiatomic FeCo alloys: Constitution, mechanical and magnetic properties," *Progress in Materials Science*, 50(7), pp. 816-880.
- [2] Sundar, R. S., and Deevi, S. C., 2013, "Soft magnetic FeCo alloys: alloy development, processing, and properties," *International Materials Reviews*, 50(3), pp. 157-192.
- [3] Popov, V., 2004, "Carbon nanotubes: properties and application," *Materials Science and Engineering: R: Reports*, 43(3), pp. 61-102.
- [4] Thostenson, E. T., Ren, Z. F., and Chou, T. W., 2001, "Advances in the science and technology of carbon nanotubes and their composites: a review," *Compos Sci Technol*, 61(13), pp. 1899-1912.
- [5] Peigney, A., Laurent, C., Flahaut, E., Bacsá, R. R., and Rousset, A., 2001, "Specific surface area of carbon nanotubes and bundles of carbon nanotubes," *Carbon*, 39(4), pp. 507-514.
- [6] Deng, C. F., Wang, D. Z., Zhang, X. X., and Li, A. B., 2007, "Processing and properties of carbon nanotubes reinforced aluminum composites," *Materials Science and Engineering: A*, 444(1-2), pp. 138-145.
- [7] Liu, Z. Y., Xu, S. J., Xiao, B. L., Xue, P., Wang, W. G., and Ma, Z. Y., 2012, "Effect of ball-milling time on mechanical properties of carbon nanotubes reinforced aluminum matrix composites," *Composites Part A: Applied Science and Manufacturing*, 43(12), pp. 2161-2168.
- [8] Mani, M. K., Viola, G., Reece, M. J., Hall, J. P., and Evans, S. L., 2014, "Fabrication of carbon nanotube reinforced iron based magnetic alloy composites by spark plasma sintering," *Journal of Alloys and Compounds*, 601, pp. 146-153.
- [9] Albaaji, A. J., Castle, E. G., Reece, M. J., Hall, J. P., and Evans, S. L., 2016, "Synthesis and properties of graphene and graphene/carbon nanotube-reinforced soft magnetic FeCo alloy composites by spark plasma sintering," *Journal of Materials Science*, 51(16), pp. 7624-7635.
- [10] Suryanarayana, C., E. Ivanov, and V. V. Boldyrev., 2001, "The science and technology of mechanical alloying" *Materials Science and Engineering A*, 304-306 pp. 151-158.
- [11] Suryanarayana, C., 2001, "Mechanical alloying and milling," *Progress in Materials Science*, 46(1), pp. 1-184.
- [12] Suryanarayana, C., and Al-Aqeeli, N., 2013, "Mechanically alloyed nanocomposites," *Progress in Materials Science*, 58(4), pp. 383-502.
- [13] Esawi, A., and Morsi, K., 2007, "Dispersion of carbon nanotubes (CNTs) in aluminum powder," *Composites Part A: Applied Science and Manufacturing*, 38(2), pp. 646-650.
- [14] Azadehranjbar, S., Karimzadeh, F., and Enayati, M. H., 2012, "Development of NiFe-CNT and Ni₃Fe-CNT nanocomposites by mechanical alloying," *Advanced Powder Technology*, 23(3), pp. 338-342.
- [15] Smart, S. K., Ren, W.C., Cheng, H.M., Lu, G.Q. and Martin, D.J., 2007, "Shortened double-walled carbon nanotubes by high-energy ball milling," *International Journal of Nanotechnology*, 4(5), pp. 618-633.
- [16] Locci, A.M., Orru, R., Cao, G. and Munir, Z.A., 2006, "Effect of ball milling on simultaneous spark plasma synthesis and densification of TiC-TiB₂ composites," *Materials Science and Engineering: A*, 434(1), pp.23-29.
- [17] Kuzumaki, T., Miyazawa, K., Ichinose, H. and Ito, K., 1998, "Processing of carbon nanotube reinforced aluminum composite," *Journal of Materials Research*, 13(09), pp.2445-2449.

- [18] Yogamalar, R., Srinivasan, R., Vinu, A., Ariga, K., and Bose, A. C., 2009, "X-ray peak broadening analysis in ZnO nanoparticles," *Solid State Communications*, 149(43-44), pp. 1919-1923.
- [19] Khorsand Zak, A., Abd. Majid, W. H., Abrishami, M. E., and Yousefi, R., 2011, "X-ray analysis of ZnO nanoparticles by Williamson-Hall and size-strain plot methods," *Solid State Sciences*, 13(1), pp. 251-256.
- [20] Osswald, S., Flahaut, E., and Gogotsi, Y., 2006, "In situ Raman spectroscopy study of oxidation of double- and single-wall carbon nanotubes," *Chem Mater*, 18(6), pp. 1525-1533.
- [21] Dresselhaus, M. S., Dresselhaus, G., Saito, R., and Jorio, A., 2005, "Raman spectroscopy of carbon nanotubes," *Physics Reports*, 409(2), pp. 47-99.
- [22] Jorio, A., Souza Filho, A. G., Dresselhaus, G., Dresselhaus, M. S., Swan, A. K., Ünlü, M. S., Goldberg, B. B., Pimenta, M. A., Hafner, J. H., Lieber, C. M., and Saito, R., 2002, "G-band resonant Raman study of 62 isolated single-wall carbon nanotubes," *Physical Review B*, 65(15), p.155412.
- [23] Zhao, X., Ando, Y., Qin, L.-C., Kataura, H., Maniwa, Y., and Saito, R., 2002, "Multiple splitting of G-band modes from individual multiwalled carbon nanotubes," *Applied Physics Letters*, 81(14), pp. 2550-2552.
- [24] Mu, M., Osswald, S., Gogotsi, Y., and Winey, K. I., 2009, "An in situ Raman spectroscopy study of stress transfer between carbon nanotubes and polymer," *Nanotechnology*, 20(33), p. 335703.
- [25] Bozorth, Richard M., "Ferromagnetism", New York, IEEE press, 2 nd edition, 1978, pp.15.
- [26] Hug, E., Hubert, O. and Guillot, I., 2000, "Effect of strengthening on the magnetic behaviour of ordered intermetallic 2% V-CoFe alloys," *Journal of magnetism and magnetic materials*, 215, pp.197-200.
- [27] Vostrowsky, A. H. O., 2005, "Functionalization of Carbon Nanotubes," *Top Curr. Chem.* , 245, pp. 193-237.
- [28] Albaaji, A.J., Castle, E.G., Reece, M.J., Hall, J.P. and Evans, S.L., 2016, "Mechanical and magnetic properties of spark plasma sintered soft magnetic FeCo alloy reinforced by carbon nanotubes," *Journal of Materials Research*, 31(21), pp.3448-3458.
- [29] George, R., Kashyap, K. T., Rahul, R., and Yamdagni, S., 2005, "Strengthening in carbon nanotube/aluminium (CNT/Al) composites," *Scripta Materialia*, 53(10), pp. 1159-1163.
- [30] Woo, D. J., Sneed, B., Peerally, F., Heer, F. C., Brewer, L. N., Hooper, J. P., and Osswald, S., 2013, "Synthesis of nanodiamond-reinforced aluminum metal composite powders and coatings using high-energy ball milling and cold spray," *Carbon*, 63, pp. 404-415.
- [31] Zhao, L. and Baker, I., 1994, "The effect of grain size and Fe: Co ratio on the room temperature yielding of FeCo," *Acta Metallurgica et Materialia*, 42(6), pp.1953-1958.
- [32] Hosoda, H., Miyazaki, S., Inoue, K., Fukui, T., Mizuuchi, K., Mishima, Y., and Suzuki, T., 2000, "Cold rolling of B2 intermetallics," *Journal of Alloys and Compounds*, 302(1-2), pp. 266-273.
- [33] Han, Q., Setchi, R. and Evans, S.L., 2016, "Synthesis and characterisation of advanced ball-milled Al-Al₂O₃ nanocomposites for selective laser melting," *Powder Technology*, 297, pp.183-192.

Figures

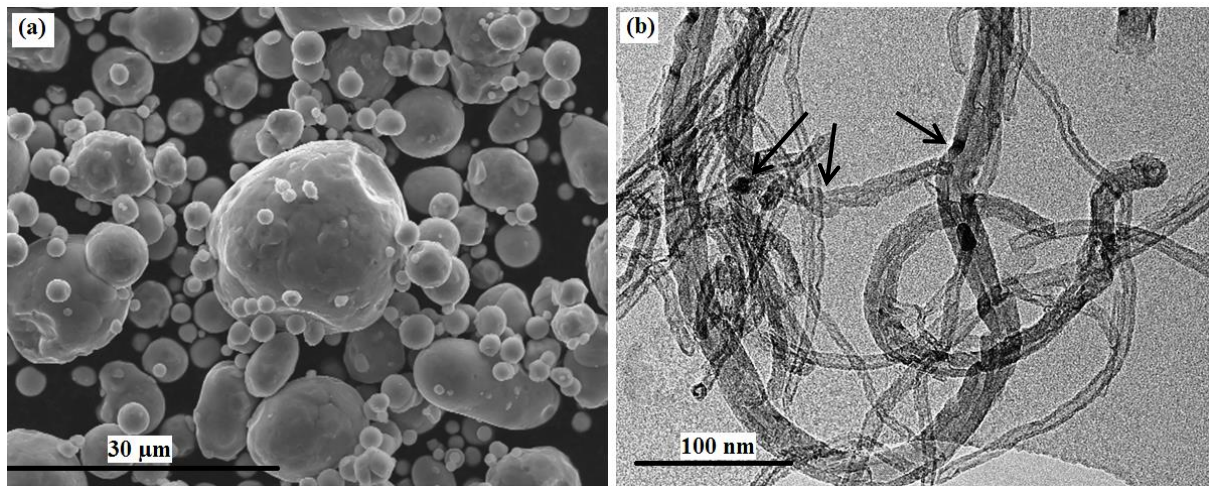


Fig.1. Morphology of as-received (a) SEM of FeCo alloy powder and (b) TEM of CNTs; arrows show damage.

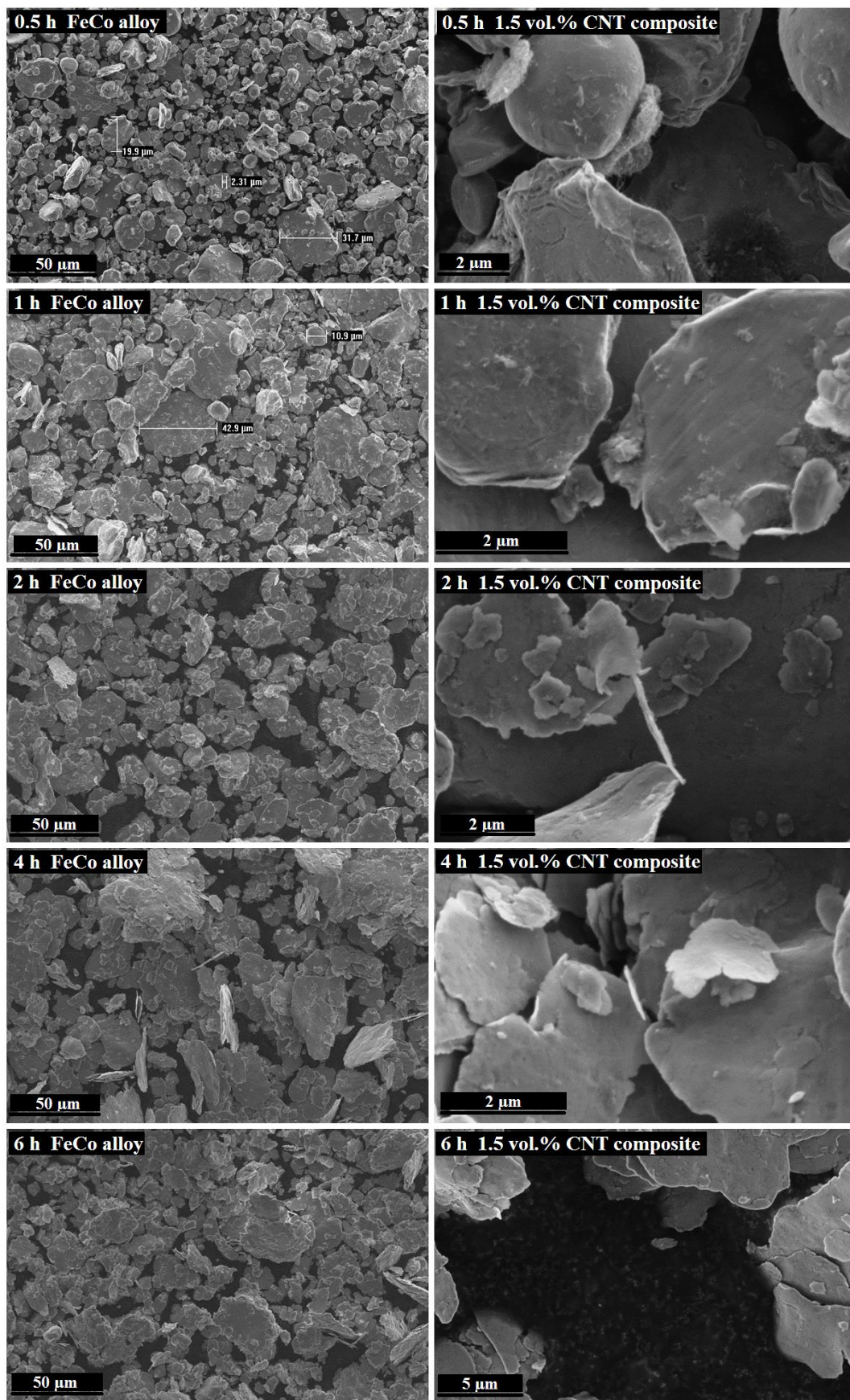


Fig.2. Surface morphology of the monolithic FeCo alloy and composite powders ball milled for the indicated ball-milling time.

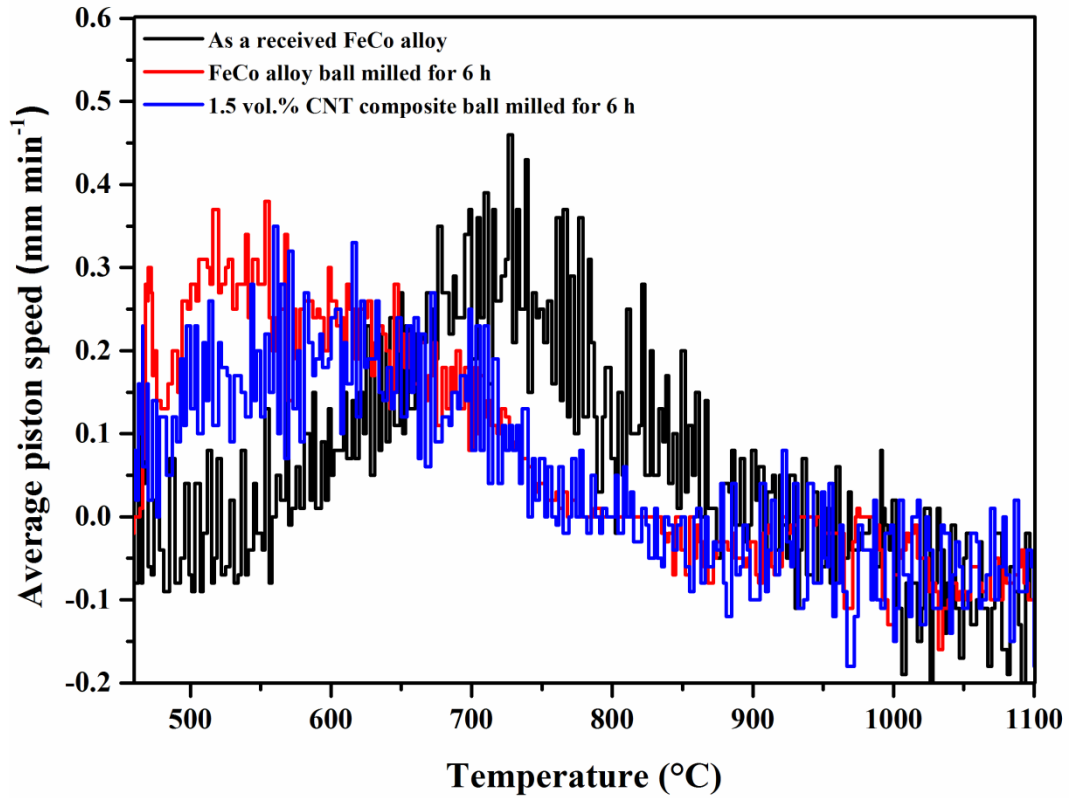


Fig.3. Change in average piston speed against temperature for the indicated materials.

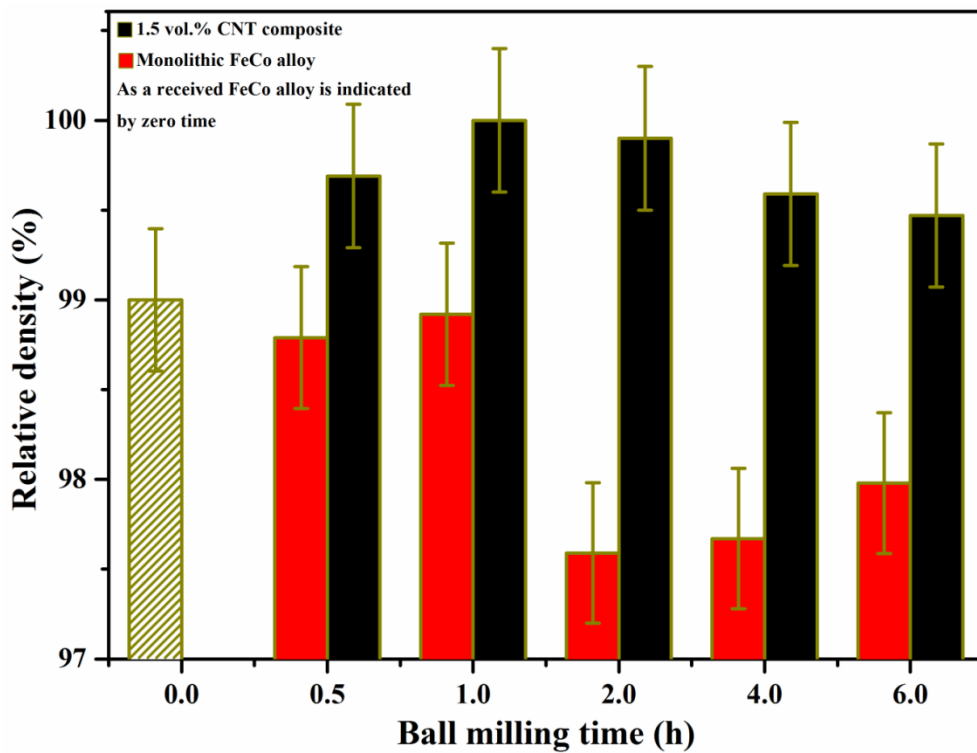


Fig.4. Variation of relative density of SPS sintered 1.5 vol. % CNT composite with ball milling time.

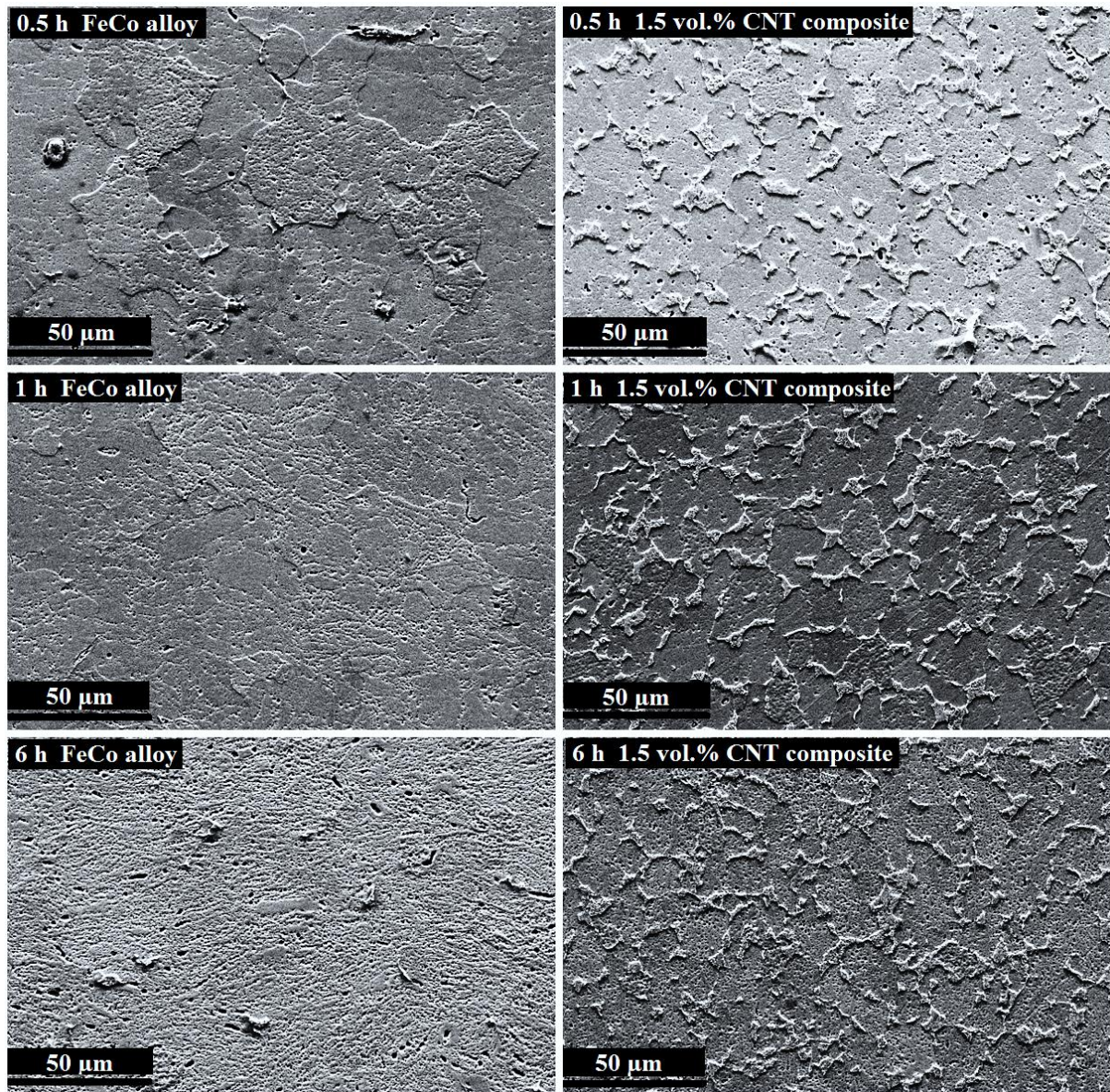


Fig.5. SEM microstructure of monolithic FeCo alloy and 1.5 vol. % CNT composite of indicated ball-milling time.

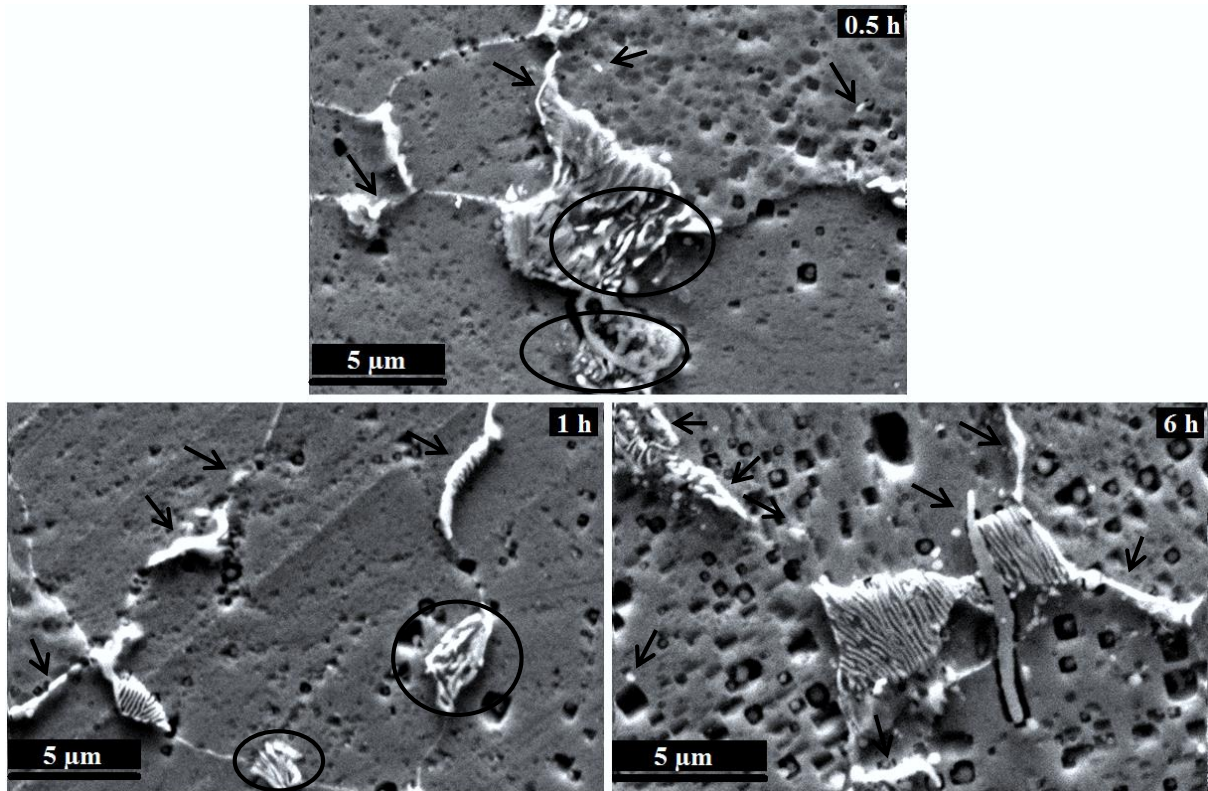


Fig.6. High-magnification SEM microstructure of 1.5 vol. % CNT composite of signified ball-milling time, the arrows indicate to single CNT, and the ellipses to agglomerated CNT.

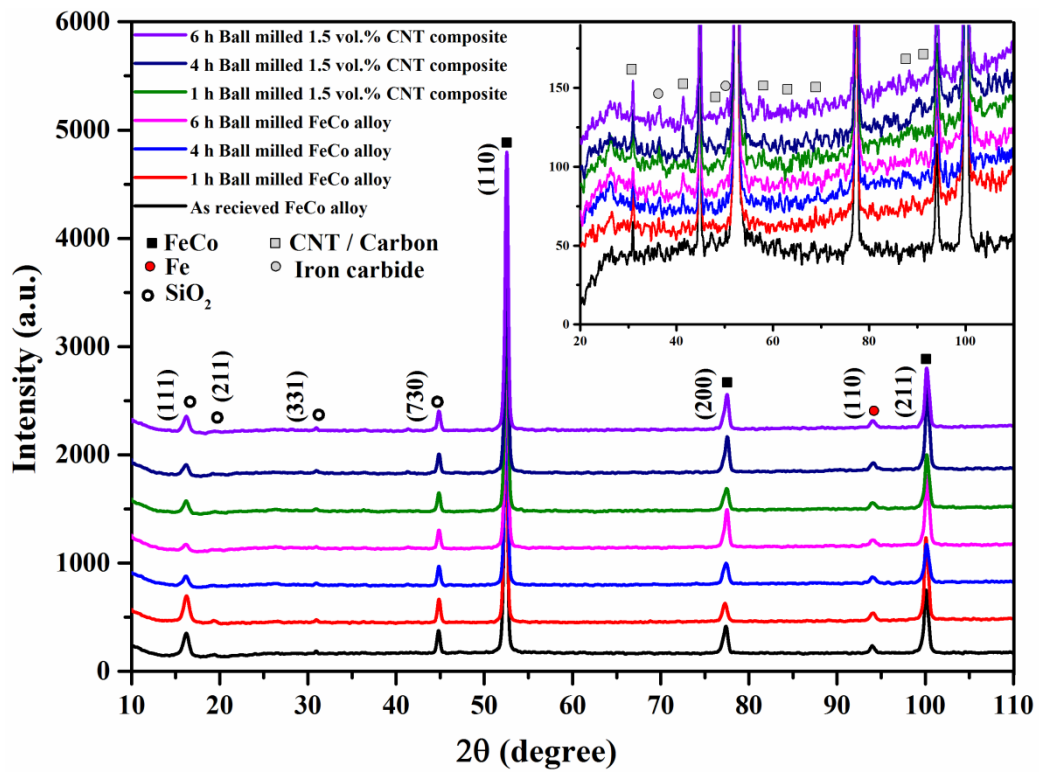


Fig.7. X-ray diffraction patterns of consolidated materials for indicated milling time.

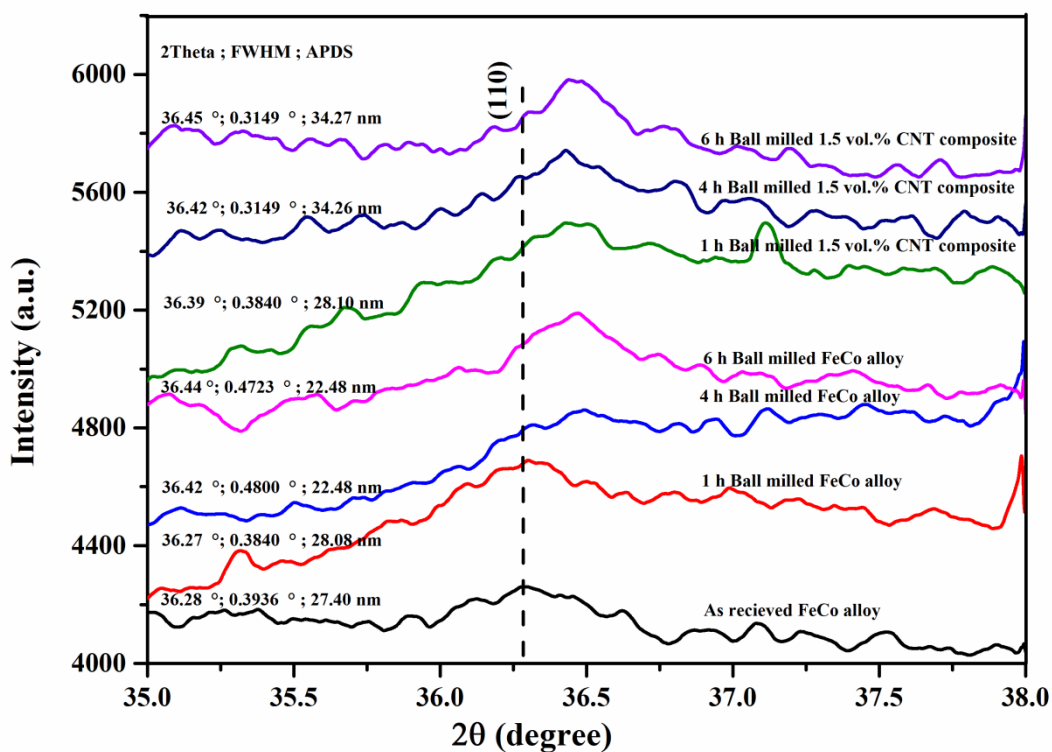


Fig.8. Slow scan XRD patterns, illustrating (100) superlattice reflections for the indicated materials, the diffraction angle (2Theta), the full width half maximum (FWHM) and the anti-phase domain size (APDS) are also displayed.

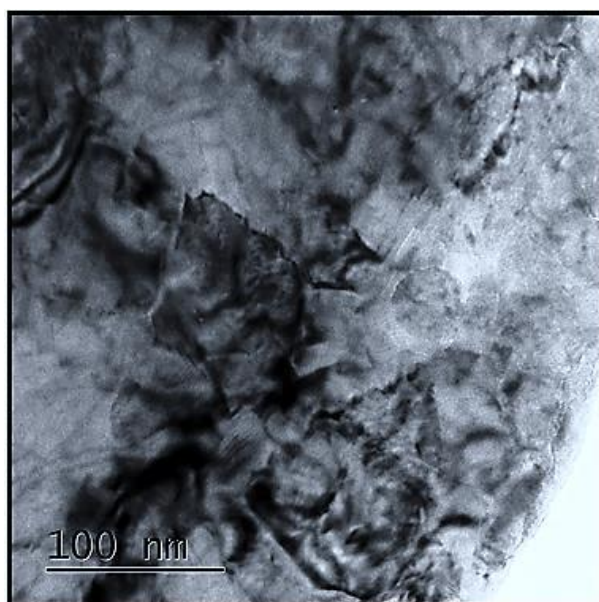


Fig.9. TEM image shows formation of a nanocrystalline structure in the powder of the monolithic FeCo alloy after ball-milling for 6 h.

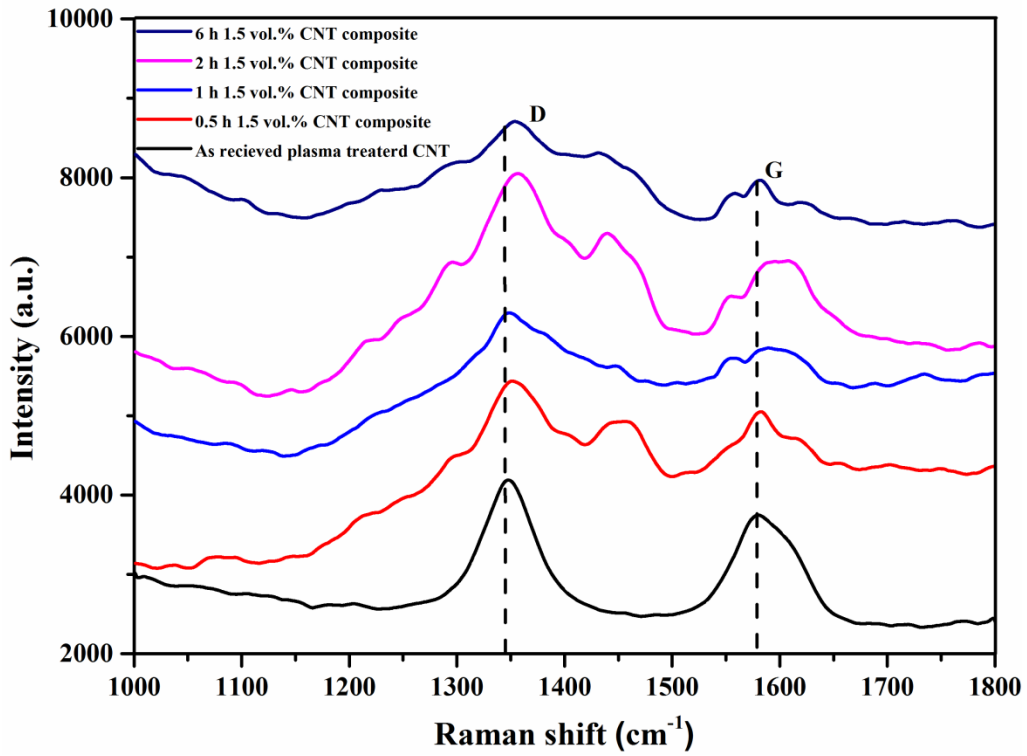


Fig.10. Raman spectra of as received CNT and 1.5 vol. % CNT composite of different ball-milling time.

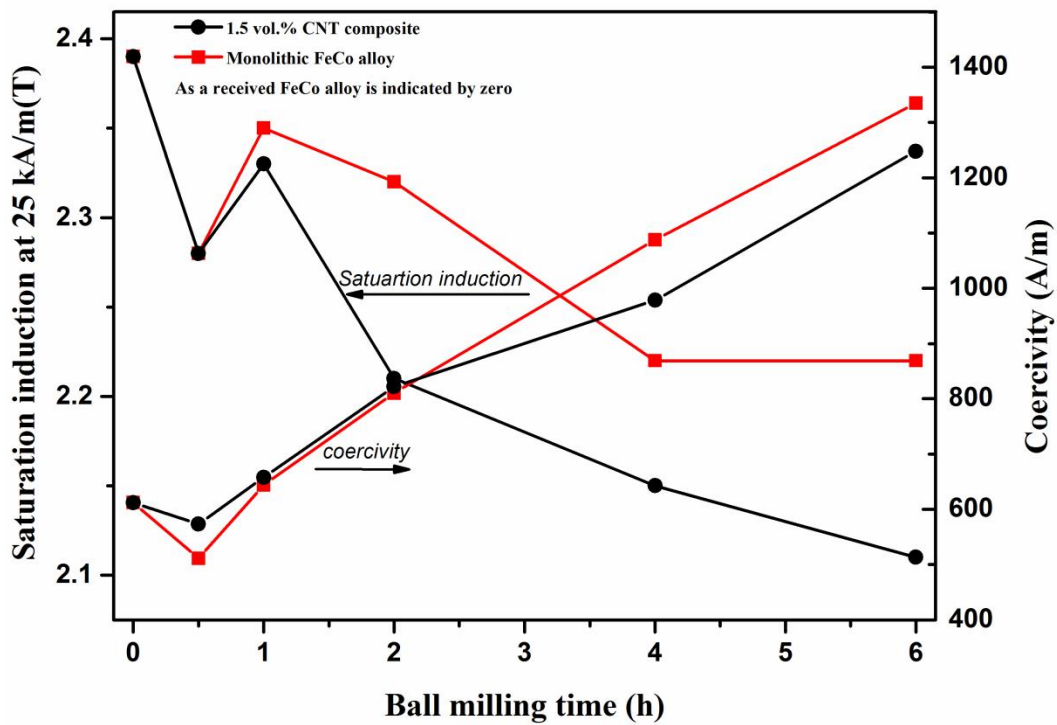


Fig.11. Summary of the magnetic properties of monolithic FeCo alloy and 1.5 vol. % CNT composite at different ball milling time.

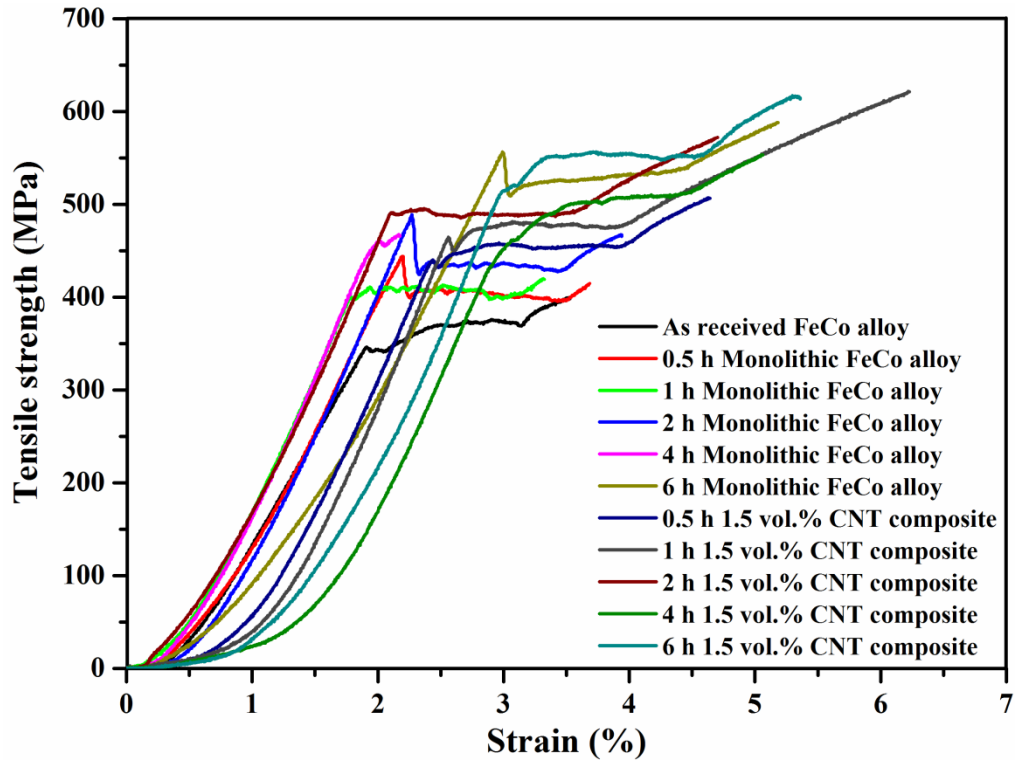


Fig.12. Tensile stress-strain curves of monolithic FeCo alloy and 1.5 vol. % CNT composite for different ball-milling time.

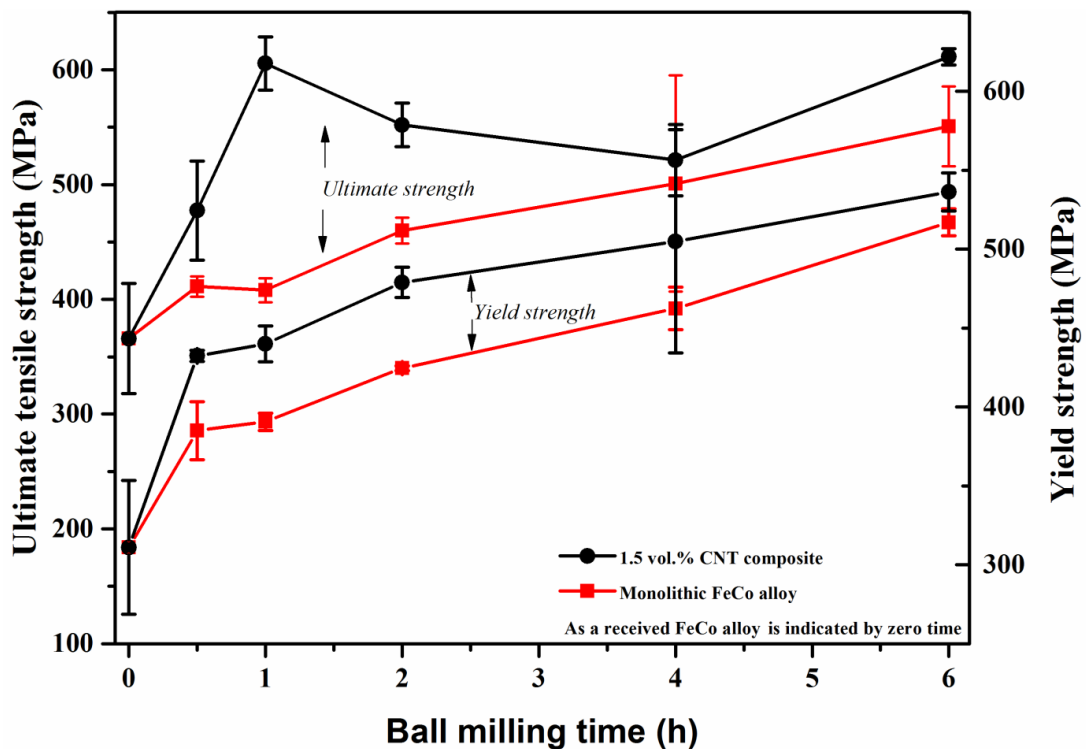


Fig.13. Ultimate tensile strength and yield strength of monolithic FeCo alloy and 1.5 vol. % CNT composite with different ball-milling time.

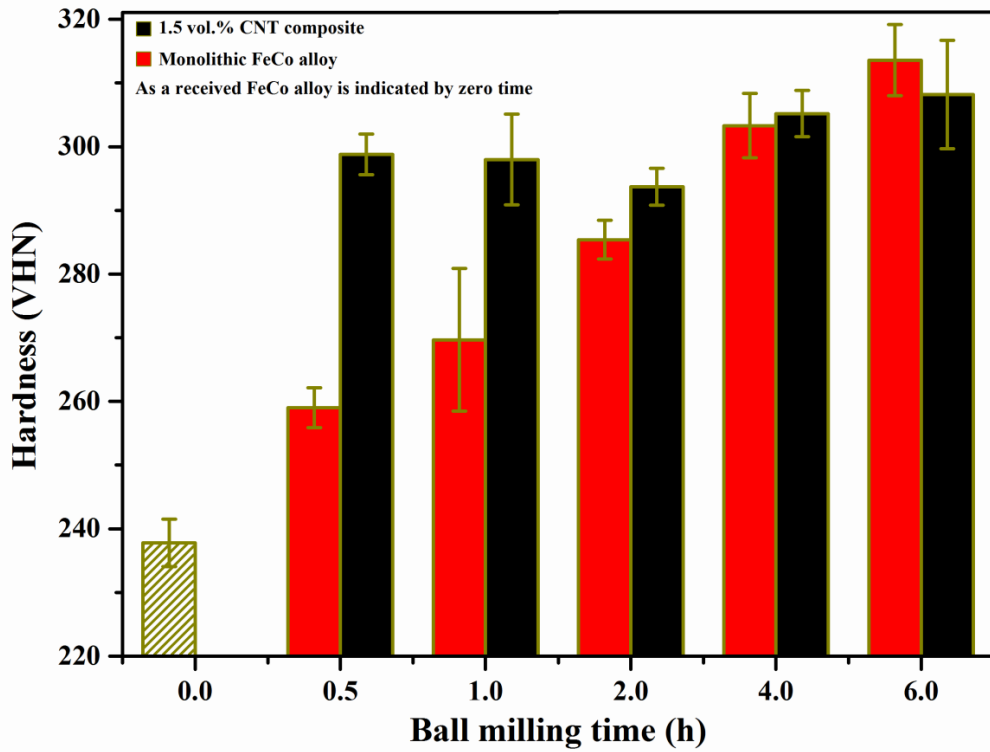


Fig.14. Changes of hardness with ball milling time of monolithic FeCo alloy and 1.5 vol. % CNT composite

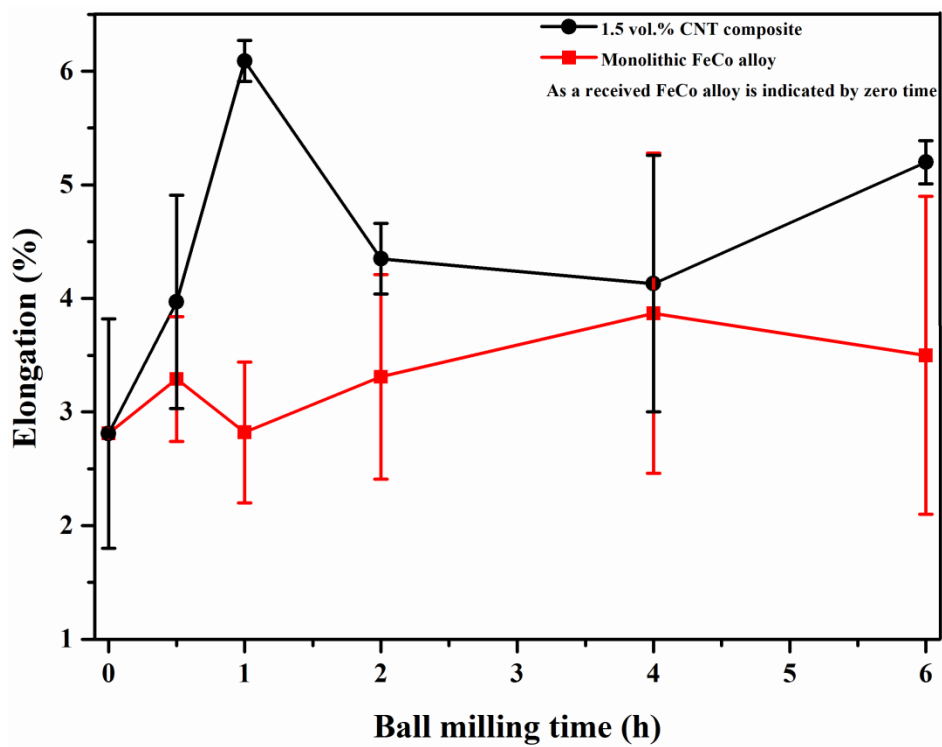


Fig.15. Elongation of monolithic FeCo alloy and 1.5 vol. % CNT composite with different ball-milling time.

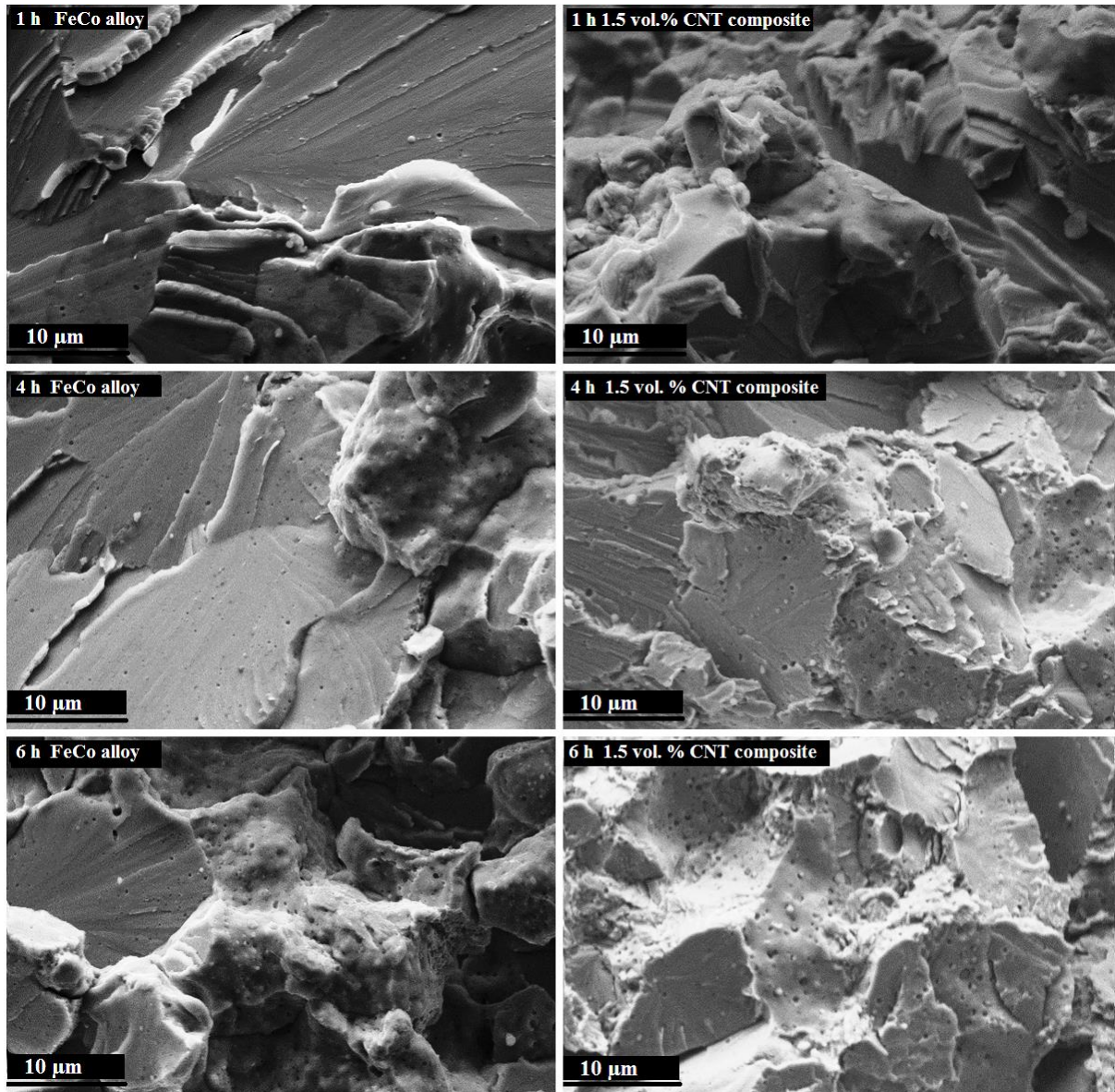


Fig.16. Fractographs of monolithic FeCo alloy and 1.5 vol. % CNT composites for indicated ball-milling times.

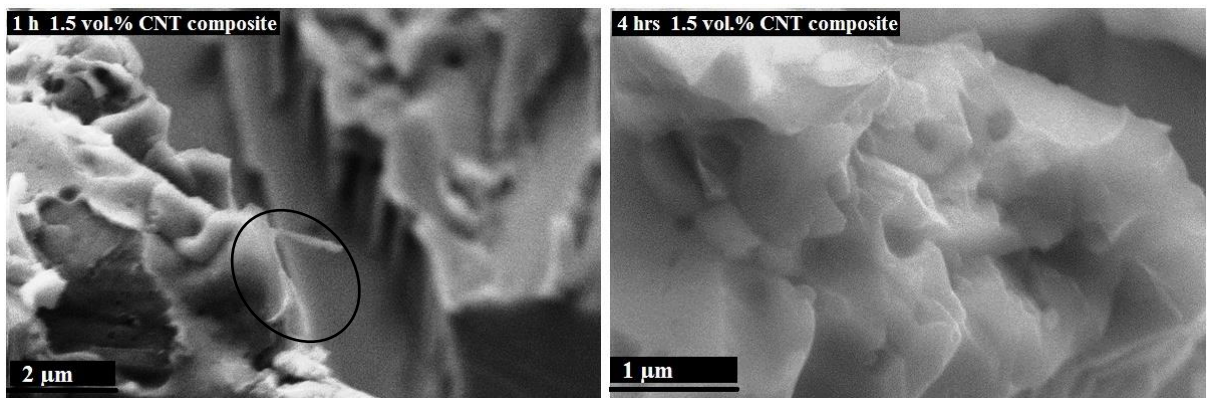


Fig.17. High magnification SEM of fracture surface of 1.5 vol. % CNT composites for indicated ball-milling times.

Tables

Table 1 Variation of particles diameter of monolithic FeCo alloy and 1.5 vol. % CNT composite with ball-milling time.

Time (h)	Average powder particles diameter after ball-milling (μm) \pm 5 %	
	FeCo alloy	1.5 vol.% CNT composite
0.5	13	4
1	19	3
2	25	10
4	34	5
6	32	6

Table 2 Grain size of monolithic FeCo alloy and 1.5 vol. % CNT composite at different ball-milling time.

Time (h)	Grain size after ball-milling (μm)	
	FeCo alloy	1.5 vol.% CNT composite
0	29.8	-
0.5	14.7	12.7
1	14.4	11.9
6	Poor densification	14.2

Table 3. Raman spectra characteristics of the as received and 1.5 vol. % CNT consolidated composites at different ball-milling times.

Milling time (h)	0	0.5	1	2	6
R= (I_D/I_G) ratio	1.11	1.03	1.04	1.09	1.09